Research Article

Springback Characteristics of Cylindrical Bending of Tailor Rolled Blanks

Li-Feng Fan [ID],[1] **Jianjun Gou,**[2] **Ge Wang,**[3] **and Ying Gao** [ID][2]

[1]*Transportation Institute, Inner Mongolia University, Hohhot 010070,*
 Inner Mongolia Engineering Research Centre for Urban Transportation Data Science and Applications, China
[2]*College of Material Science and Engineering, Hebei University of Science and Technology, Shijiazhuang 050018, China*
[3]*National Engineering Research Centre for Equipment and Technology of Cold Strip Rolling, Yanshan University,*
 Qinhuangdao 066004, China

Correspondence should be addressed to Li-Feng Fan; fanlifeng@imu.edu.cn

As a new type of variable thickness sheet structure, the TRB (tailor rolled blank) has good prospects for the development of lightweight materials in the automotive industry. However, springback is a key issue in production. Research on TRB springback characteristics has great significance for further applications due to variations in the sheet thickness and gradient distribution of the material mechanical properties. In this study, the springback characteristics of TRBs were investigated by means of the finite element code ABAQUS/USDFLD and experiments taking cylindrical bending as an example. The results showed that the cylindrical bending process of the TRB gradually evolved from three-point bending to four-point bending and, finally, to multipoint bending. At same time, the gradient of the thickness leads to the nonuniform longitudinal distribution of the von Mises stress. On the contrary, larger bending angles can be achieved by reducing R and improving R_d, but t/T has little effect on the bending angles. In terms of the influence of springback, increasing R_d and reducing R and t/T can lead to a smaller springback angle. This project provided an important opportunity to advance the understanding of TRB springback characteristics.

1. Introduction

Energy savings and environmental protection requirements necessitate lightweight designs for cars. Automobile body covering parts made of tailor rolled blanks (TRBs) can help reach these goals. TRBs are manufactured by means of a flexible rolling process. In this production process, the sheet thickness is obtained by controlling the gaps between the working rollers. Reports on the TRB manufacturing process are well represented in the literature [1–4]. In TRB applications, one of the main problems is the springback problem caused by elastic recovery in the formation process. Moreover, TRBs with variations in sheet thickness and gradient distributions of mechanical properties have special springback characteristics. Therefore, it is necessary to investigate the springback characteristics of TRBs and further develop their properties.

Many research approaches, including analytical, semi-analytical, and seminumerical methods as well as the finite element method (FEM), are used to predict the springback of the bending process. H. J. Jiang and Dai[5], N. Nanu and Brabie [6], and Yang et al. [7] predicted springback by using analytical models. Quilliec et al. [8], Lee et al. [9], and Panthi and Ramakrishnan [10] proposed semianalytical approaches for springback prediction. The research results from the analytical approach have poor calculation accuracy because of the simplification of the mathematical model. Fortunately, the finite element method can overcome such a disadvantage.

Chongthairungruang et al. [11] investigated the springback effect of an advanced high-strength dual-phase steel by applying experimental and numerical simulations. Guo et al. [12] performed a numerical simulation to research the springback in the formation of advanced high-strength

steel sheets. Kim and Kimchi[13] established numerical modelling for springback predictions by considering the variations in the elastic moduli of stamped advanced high-strength steels (AHSSs). However, it is difficult to calculate the springback of TRBs by the FEM because TRBs have special material properties due to variations in the sheet thickness. Zhang et al. [14] and Zhang et al. [15] conducted numerical simulations of the mechanical properties of TRBs by discrete methods. For a more precise description of the special material properties of TRBs, a constitutive relationship integrating the variation in sheet thickness for TRBs is provided based on digital image correlation (DIC) tests, and the user subroutine USDFLD programmed in FORTRAN is used to implement the gradients of the mechanical properties with the TRB thickness in the finite element model in this paper.

In past years, many studies have been performed on the formation behaviour of TRBs with the FEM. Zhang et al. [16] investigated the springback characteristics of the formation of TRB U-channels. Meyer et al. [17] studied the formability of TRBs in deep drawing processes. Kim et al. [18] studied the hot formation of an Al6061 TRB-integrated heat-treatment process to improve the formation accuracy. Shim et al. [19] analysed springback predictions for a TRB in a partial heating process considering its thickness and temperature variation. Lu et al. [20] investigated the springback behaviours of TRBs of high-strength steels, including CR340, DP590, and Q&P980, together with light aluminium after U-channel forming. Therefore, the springback of a TRB is not only related to the formation process and material properties but also affects the die structure.

To easily reveal the springback characteristics of TRBs and simplify the formation process, a cylindrical bending process that served as the Numisheet 2002 benchmark bending problem was chosen as the research object. In this process, TRBs experience complex deformation, including multipoint bending, covered bending operations, and reverse bending. Until now, there have been few studies on the formation process and the effects of cylindrical bending die configurations on the springback characteristics of TRBs. Therefore, the aim of this work is to investigate the special springback characteristics of TRBs by means of a cylindrical bending process.

The remainder of this study is organized as follows: Section 2 describes the material used, constitutive model of the TRB, verification of the constitutive model by DIC and USDFLD, simulation of the cylindrical bending of the TRB, and validation of the simulation. Section 3 investigates the deformation characteristics of the cylindrical bending of TRBs and the effects of the formation parameters on the springback from the cylindrical bending of TRBs. Section 4 summarizes the conclusions.

2. Material and Experiments

2.1. Material.
The experimental material used in this paper is HC340LA steel produced by Northeast University. The main chemical components are $w(C) = 0.07\%$, $w(Si) = 0.195\%$,

$w(Mn) = 0.808\%$, $w(P) < 0.032\%$, $w(S) < 0.06\%$, $w(Nb) = 0.03\%$, and $w(Ti) = 0.03\%$. The metallographic structure is shown in Figure 1, illustrating that the metallographic structure is composed of equiaxed ferrite grains with uniformly dispersed cementite particles.

2.2. Constitutive Model of TRB and Verification

2.2.1. DIC Tests.
Tensile tests are performed on plate-shaped specimens in accordance with the Chinese national standard GB/T 228.2—2015 with the objective of investigating the deformation behaviour at different thicknesses. The true stress-true strain field of a TRB with the variation in the sheet thickness was constructed by uniaxial tension tests and the Lagrange polynomial interpolation method in the literature [14]. In this study, specimens are used for tensile tests (as shown in Figure 2).

To test and calculate the displacement and strain of a TRB in the tensile deformation process, a high-quality speckle sample is machined. For the TRB tensile test, the key test area is the transition region of the specimens, which is precisely 100 mm. Therefore, this region is specified as the area for the DIC analysis, and a parametric study is used to determine effective subset and step sizes for the experiments. The main techniques used in the DIC test combine the digital speckle correlation method and binocular stereo vision technology. The strain data and displacement information are visualized using DIC software. The load is obtained from an universal tensile testing machine. Finally, the results synchronizing the DIC and tensile tests are used to establish the TRB constitutive model. The universal tensile testing machine used for the tensile tests coupled with the DIC tests is shown in Figure 3.

2.2.2. Constitutive Model.
The constitutive model is assumed to be isotropic without considering the anisotropic behaviour of the material. Generally, from experiments with plate specimens of the same thickness under tension, the function $\sigma_{true}(\varepsilon_{plastic})$, which can express the true stress-plastic strain relationship, is obtained according to equations (1)–(6):

$$\sigma_{true} = \frac{F}{A}, \tag{1}$$

$$\varepsilon_{true} = \ln\left(\frac{A_0}{A}\right), \tag{2}$$

$$\varepsilon_{plastic} = \varepsilon_{true} - \frac{\sigma_{true}}{E}, \tag{3}$$

where F is the current tensile load, A_0 is the initial undeformed cross section of the specimen, and A is the current cross section of the specimen.

As the thickness in the TRB varies, the transition zone is divided into several parts, and each part is equivalent to a plate of equal thickness. Therefore, the following formula can be obtained for a discrete part:
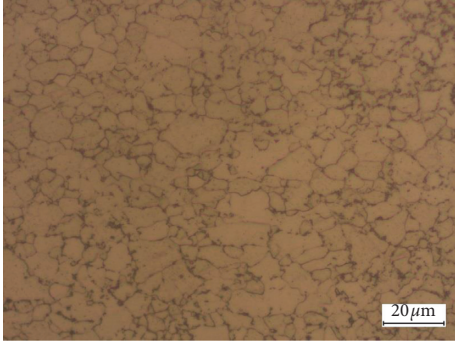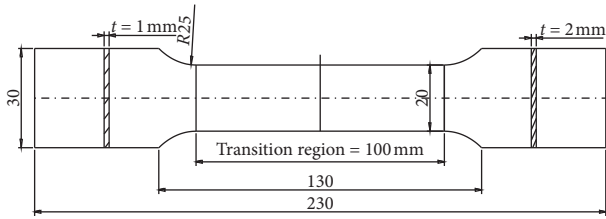
FIGURE 1: Metallographic structure.
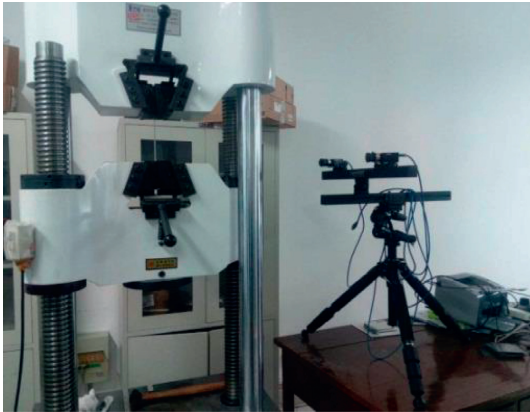

FIGURE 2: Plate tensile specimens.

FIGURE 3: Universal tensile test machine coupled with DIC test equipment.

$$\sigma_{\text{true}}^i = \frac{F}{A_i}, \tag{4}$$

$$\varepsilon_{\text{true}}^i = \ln\left(\frac{A_{0i}}{A_i}\right), \tag{5}$$

$$\varepsilon_{\text{plastic}}^i = \varepsilon_{\text{true}}^i - \frac{\sigma_{\text{true}}^i}{E_i}, \tag{6}$$

where σ_{true}^i is the true stress for the discrete part, $\varepsilon_{\text{true}}^i$ is the true strain for the discrete part, $\varepsilon_{\text{plastic}}^i$ is the plastic strain for the discrete part, A_{0i} is the initial undeformed cross section for the discrete part, A_i is the current cross section for the discrete part, and E_i is the elastic modulus for the discrete part.

According to the testing techniques proposed here, the curves of true stress-plastic strain with plate thickness are shown in Figure 4.
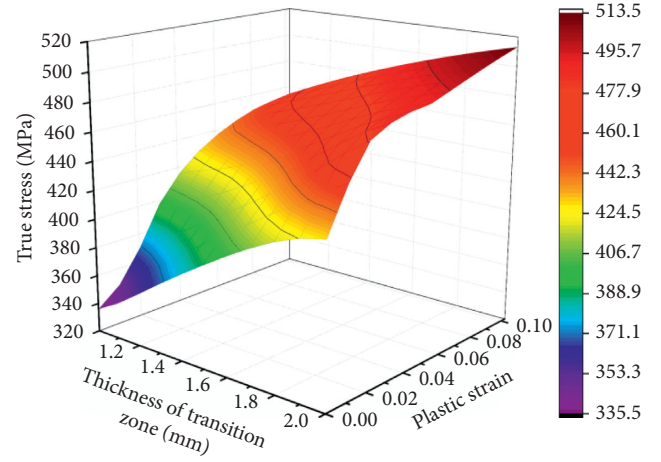

FIGURE 4: Curves of true stress-plastic strain with TRB thickness.

According to the curves of the true stress-plastic strain, hardening and nonuniform behaviour can be identified from the experimental data. Therefore, the hardening behaviour and nonuniform behaviour are summarized as follows:

(1) The strain hardening effect is significant when the material enters the plastic stage since the true stress-plastic strain curve is obviously convex. In addition, the true stress increases with the strain for different thickness conditions.

(2) The true stress-plastic strain curve increases with decreasing thickness from the DIC test data in Figure 3, and the yield strength increased 27.4%, from 335.9 MPa to 428 MPa; hence, the nonuniform behaviour due to varying TRB thickness is extremely significant.

2.2.3. Verification. To verify the constitutive model of the TRB, it is essential to perform finite element analysis of the TRB tensile tests. Based on the parameters extracted in Section 2.2, a static, general, and elastoplastic large deformation FE analysis is performed to model the above-mentioned specimens. The nonlinear commercial software ABAQUS is used for the FE analysis, in which the user subroutine USDFLD programmed in FORTRAN is used to implement the gradients in the mechanical properties with the TRB thickness in the finite element model. The characteristics of the mechanical properties of the TRB are defined by the correlation between the X coordinates and the thickness of the TRB. Eight-node linear brick reduced integration elements are used, and displacement conditions are imposed at the end plane of the specimen to simulate the motion of the testing machine crosshead. In this study, good convergence is achieved by using a large number of elements. The model of the TRB is composed of 14080 nodes and 11340 elements, as shown in Figure 5, in which the element size is 2 mm.

A sensitivity analysis of the mesh was performed by 1 mm, 2 mm, 3 mm, 4 mm, and 5 mm element size in Figure 6. It has little effect on the results of the analysis. The
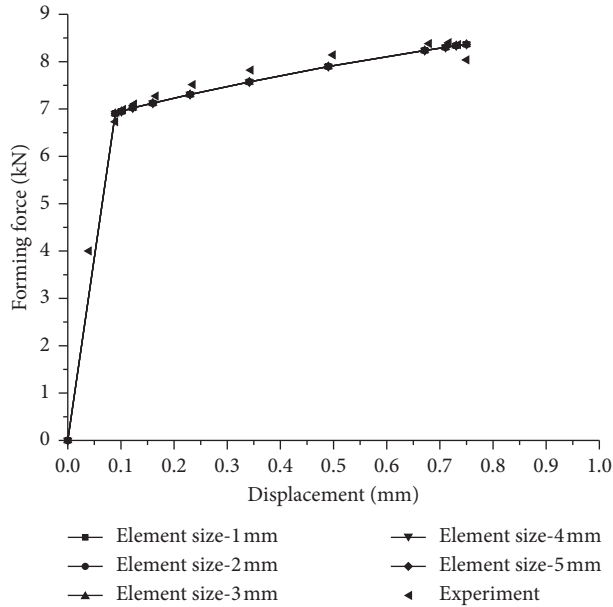
FIGURE 5: The smooth round bar specimens.

FIGURE 6: Displacement-forming force curves for TRB specimens from FEM and experiment.

numerical results were then validated by experiments, and good agreement was observed between the results, as indicated by the displacement-forming force curves in Figure 6. Therefore, the material characterization performed in Section 2 is accurate.

2.3. Cylindrical Bending of TRB

2.3.1. Experiment. The cylindrical bending of the TRB problem investigated in this study is shown in Figure 7. The geometric shape and position conditions are modified based on the Numisheet 2002 benchmark bending problem. The TRB transition region of the sheet is the same as that used in DIC and tensile tests. Its dimensions are $L = 100$ mm, $W = 100$ mm, and $t = 1$ mm~2 mm. The geometric characteristics of the cylindrical bending of the TRB experiment are as follows: die radius $R_d = 25$ mm, die corner radius $R = 4$ mm, and punch radius $R_p = 23$ mm.

Cylindrical bending experiments on the TRB are carried out with a universal tensile testing machine to evaluate the accuracy of the proposed simulation model. The experimental data, including the bending angle during loading and bending angle after unloading, are measured using a 3D scanner measuring machine. A scanner on the measurement equipment is used to construct a space surface by binocular vision technology. Therefore, the first measurement step is to obtain the bending angle during loading, α loading, when the punch moves down to the specified location. The second measurement step is conducted by measuring α unloading
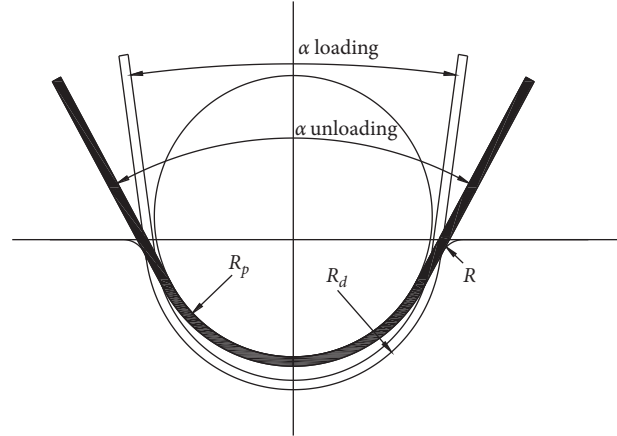

FIGURE 7: Cylindrical bending of TRB.

when the punch moves up. Finally, the springback values of the formed TRB sheets can be calculated by difference analysis. An illustration of the bending angle during loading and after unloading is shown in Figure 7.

2.3.2. Simulation of Cylindrical Bending of TRB. To investigate the springback characteristics of the cylindrical bending of the TRB, the simulation of the formation process is carried out by the finite element code ABAQUS with a standard general solver. The moulds are set as analytical rigid bodies because the die and punch deformation is ignored, and the TRB sheet is regarded as a deformable part. According to the literature [17], the Coulomb friction model can be applied to describe the friction of interacting surfaces. A frictional coefficient of $\mu = 0.1$ is used in the simulation model. During the simulation of the TRB formation process, the die is fixed, and the punch vertically applies a load on the TRB sheet to achieve a cylindrical bending process. In the springback step, the punch is moved up to accomplish springback analysis. Throughout the entire calculation process, the nonlinear effects are considered in each analysis step (i.e., the —on‖ case of Nlgeom). Many conditions, including the displacement conditions, unit partitioning techniques and boundary conditions, are used in the finite element model. The sheet in the model is meshed with 3200 linear brick elements with 0.2 mm element size through the sheet thickness and 5 mm element size through the other directions. In order to consider the results of mesh sensitivity for numerical simulation of the bending test, the sheet in the model is remeshed with 80000 elements with 0.2 mm element size through the sheet thickness and 1 mm element size through the other directions. Comparing the two models, the results show that the maximum difference of springback angle is only 0.1355°. So, it has little effect on the results of mesh sensitivity for numerical simulation. Therefore, the first mesh scheme is still adopted to save the computational cost in this paper. Reduced integration and hourglass control are also applied. Figure 8 illustrates the mesh generation of the sheet in the present study. The presented constitutive model of the TRB is utilized in
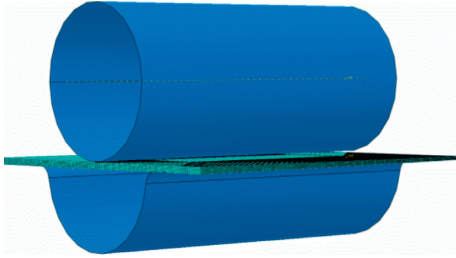
Figure 8: FEM of cylindrical bending of TRB.

simulation by ABAQUS user subroutine USDFLD, similar to the above tensile test of the TRB.

2.3.3. Cylindrical Bending of TRB FEM Validation.

2.3.3. Cylindrical Bending of TRB FEM Validation. In this section, verification of the cylindrical bending simulation is achieved in Figures 9–11. Therefore, numerical simulation of the cylindrical bending experiments in the above section is carried out, and a comparison between the measured and simulated bending angles is shown in Figures 10 and 11. The results for both bending angles agree well for the same thickness distribution. The maximum error for springback angles in the simulation is approximately 4% in Figure 11. The proposed simulation model for the TRB predicts both bending angles with high accuracy.

3. Results and Discussion

3.1. Deformation Characteristics of Cylindrical Bending of TRB. After the verification of the finite element model, the cylindrical bending characteristics, such as the stress/strain distribution and deformation characteristics, are investigated. As seen from Figures 12(a)–12(e), the loading step of cylindrical bending can be divided into five phases:

(1) The thick side of the TRB first experiences three-point elastic bending; then, the thin side gradually deforms with the thick side

(2) With increasing bending curvature, the outer layer of the TRB gradually yields, and the three-point bending evolves into elastic-plastic deformation

(3) When the curvature of the TRB is greater than the curvature of the cylinder, the contact point moves to both sides, and the three-point bending transforms into four-point bending

(4) As the TRB bending midpoint reaches the bottom of the die, multipoint bending evolves

(5) Unloading and springback occur

The relationship between the forming force and die displacement is shown in Figure 12(f). First, the forming forces are linear with the displacement under elastic deformation. Then, the forming forces increase slowly as the blank begins to yield. Next, pure sliding of the blank between the die and the punch occurs. Finally, the forming forces increase significantly at a die displacement of 25 mm for multipoint bending, which corresponds to the maximum bending of the blank.
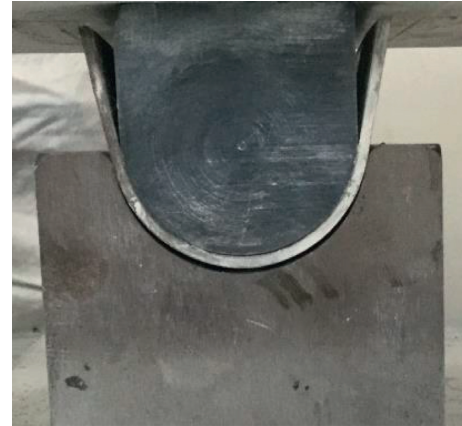

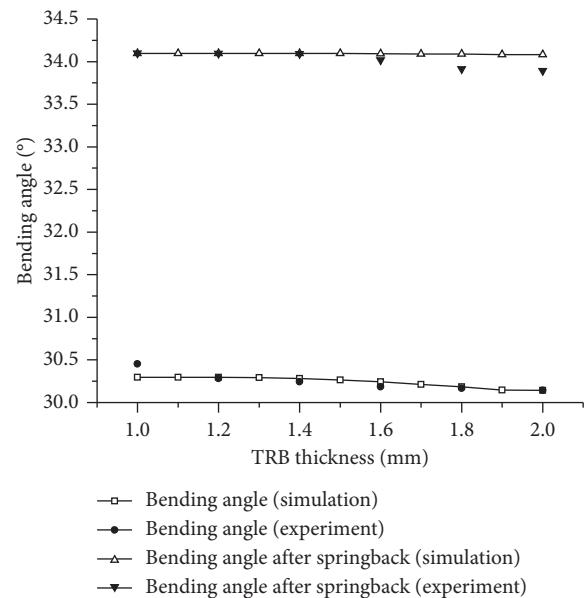Figure 9: Experiment on cylindrical bending of TRB.

Figure 10: Comparison between the measured and simulated bending angles.

Figures 13(a)–13(d) show the von Mises stress distributions of the outer layer obtained from the cylindrical bending of the TRB at different displacements during the loading process. It can be seen from the figure that the von Mises stress in the thick area is higher than that in the thin area. At the same time, the bending process gradually evolves from three-point bending to four-point bending and finally to multipoint bending. The present process has significant evolutionary stress characteristics. The analysis of the stress distribution at different thickness zones (1 mm, 1.2 mm, 1.4 mm, 1.6 mm, 1.8 mm, and 2 mm) can be seen in Figure 13(e), revealing that the curve of the von Mises stress at the 2 mm thickness zone is different from those at the other positions. The greater the thickness is, the greater the stress value is. There is a peak in the sheet and the mould contact position stress, which is directly affected by the forming force from the mould. The bottom of the curve is generally the sheet metal and mould noncontact position.
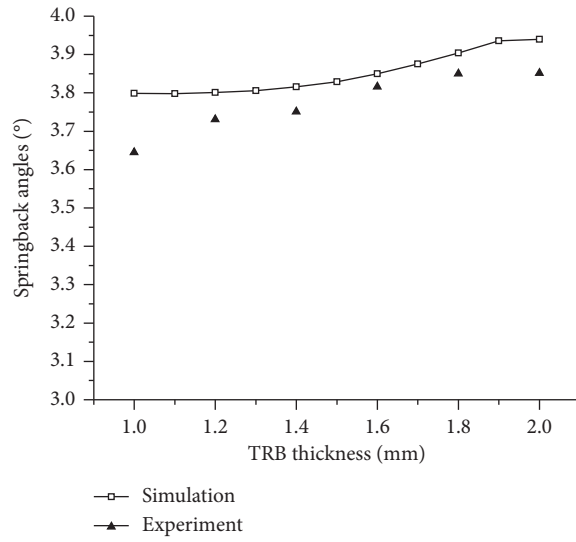
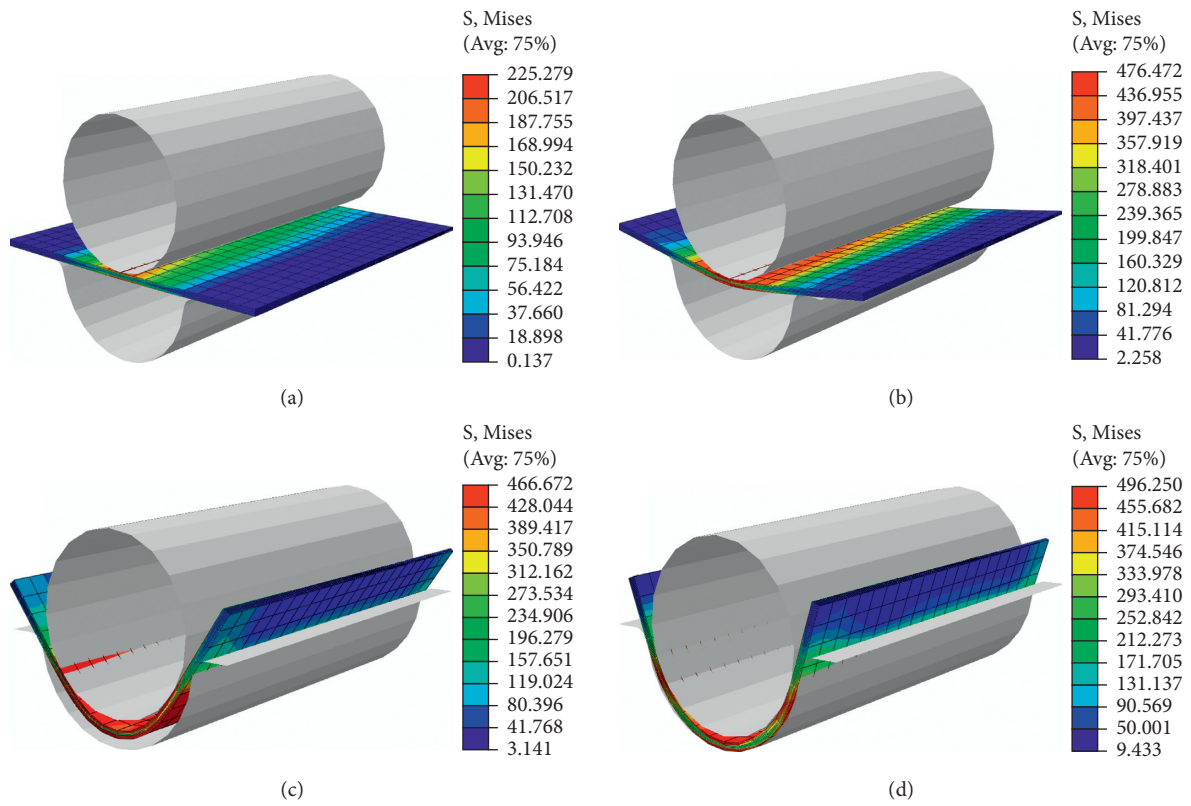FIGURE 11: Comparison between the measured and simulated springback angles.

(a)

(b)
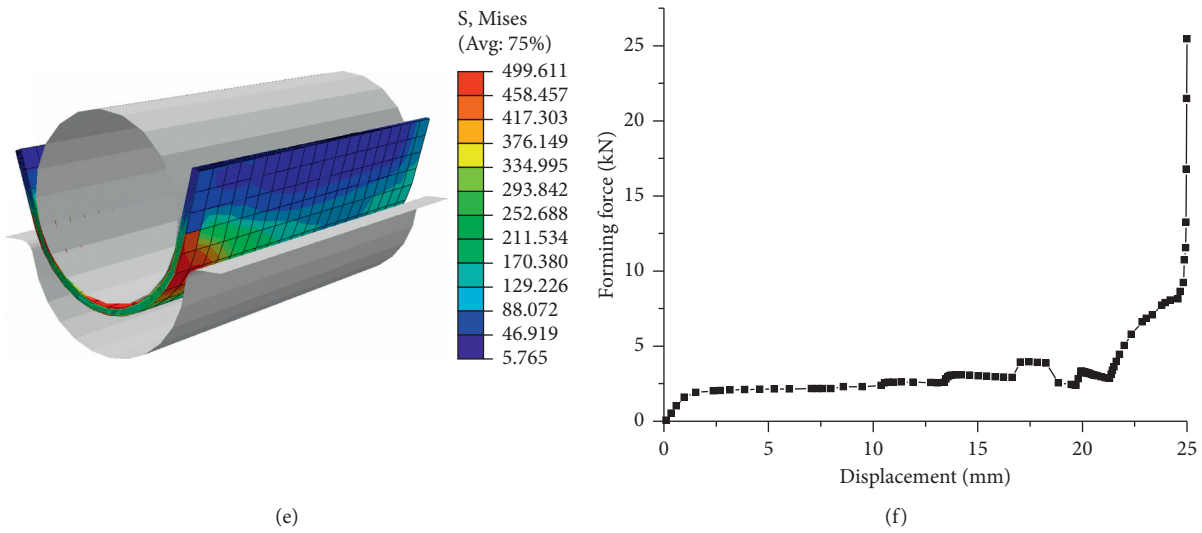

(c)

(d)

FIGURE 12: Continued.

(e)

(f)

FIGURE 12: Deformation characteristics of cylindrical bending TRB: punch displacement (a) at $h = 0.349$ mm, (b) at $h = 3.86$ mm, (c) at $h = 19.93$ mm, (d) at $h = 23.79$ mm, and (e) after unloading; (f) displacement-forming force curves.
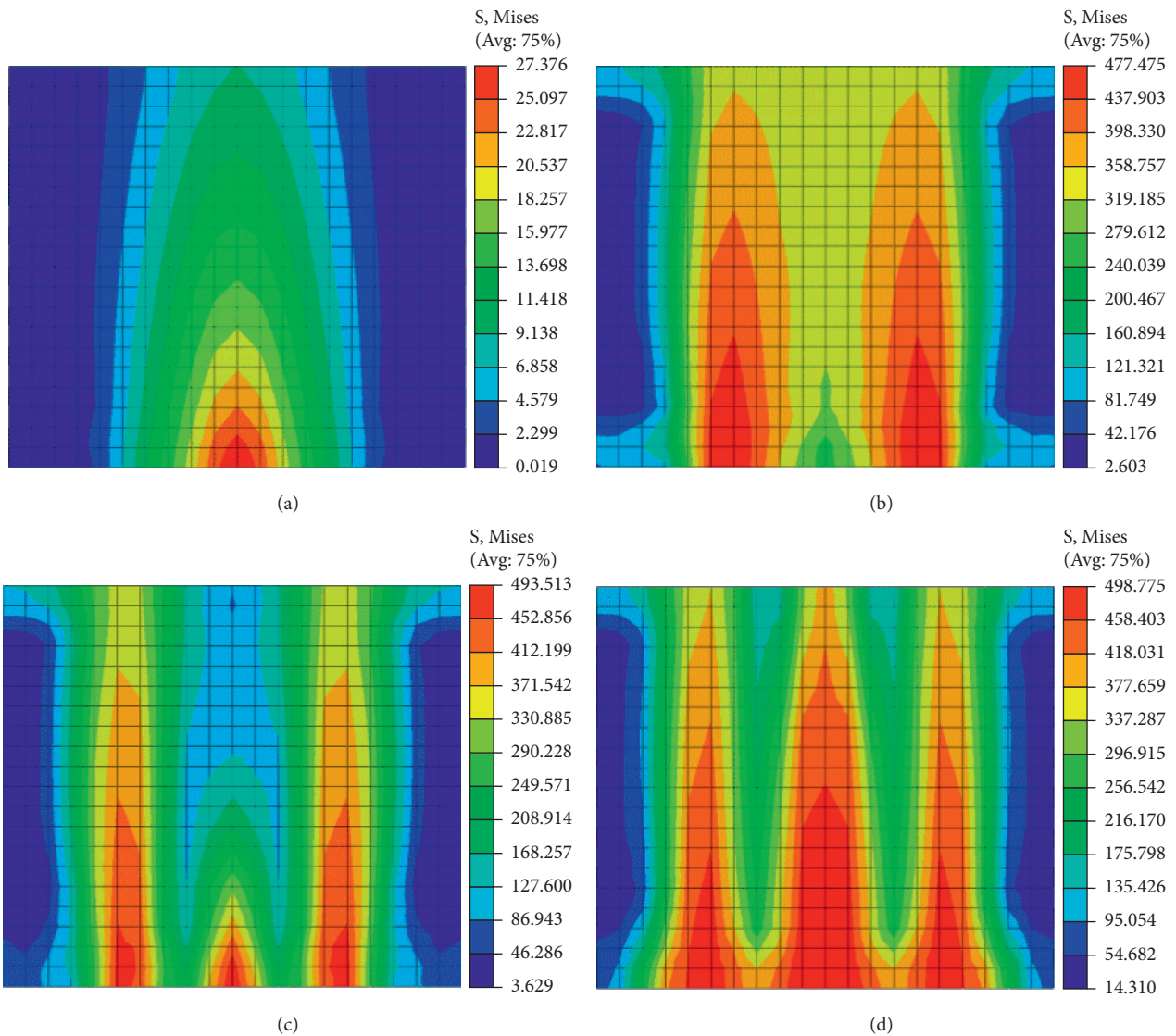

(a)

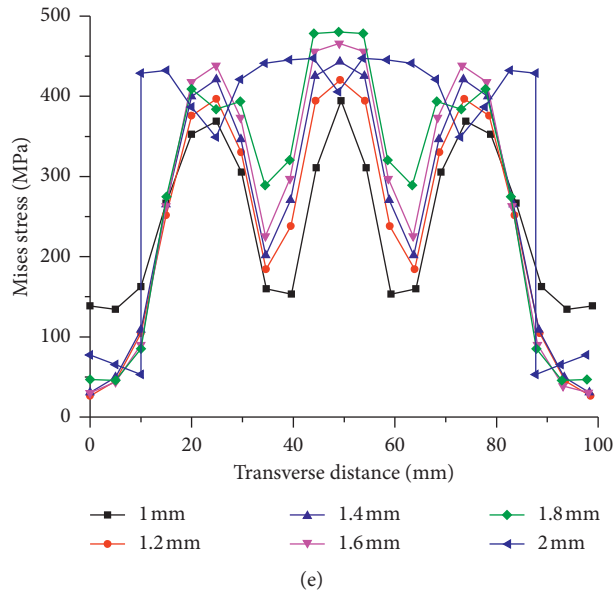

(b)

(c)

(d)

FIGURE 13: Continued.

(e)

FIGURE 13: Von Mises stress distributions of the outer layer during the loading process: von Mises stress distribution at (a) $h = 2.37$ mm, (b) $h = 21.51$ mm, (c) $h = 22.34$ mm, (d) $h = 24.83$ mm, and (e) $h = 24.83$ mm.
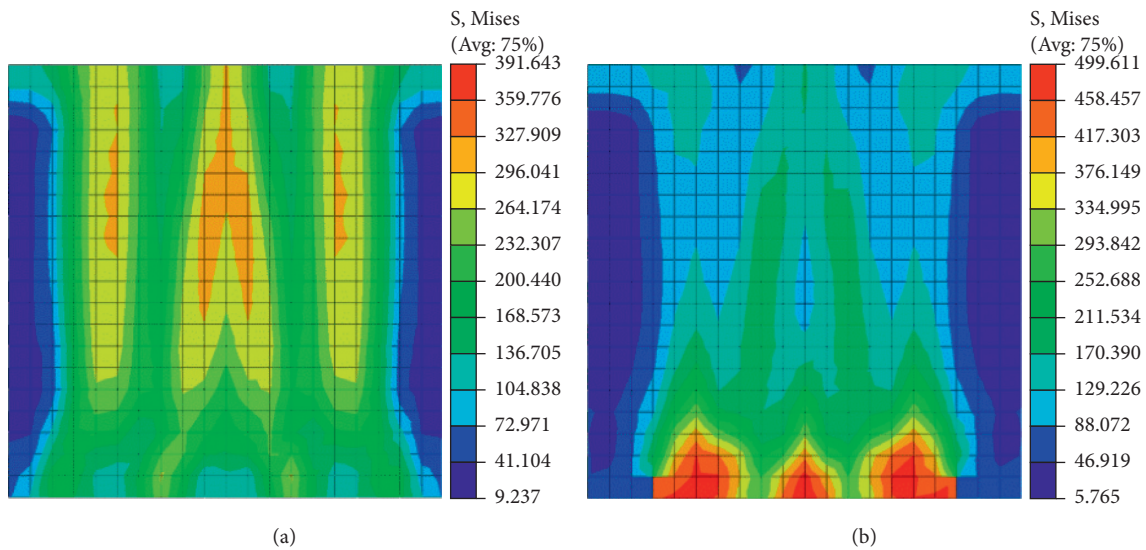

FIGURE 14: Von Mises stress distributions in the outer layer during the springback process: von Mises stress distribution during the unloading process at (a) $h = 2.83$ mm (b) and $h = 22$ mm.

Based on the above discussion, the deformation in the formation process of the cylindrical bending of TRB is consistent with that of traditional cylindrical bending, and the gradient in the thickness leads to the nonuniform longitudinal distribution of the von Mises stress.

In this study, the blank is allowed to release elastic energy incrementally as the punch is gradually moved up. Figure 14(a) shows the von Mises stress distributions of the sheet during the springback process at a stage of 9% of the assigned punch displacement. It can be seen from the figure that the maximum von Mises stress transfers from the thick zone region to the thin zone region, mainly because the springback process is equivalent to reverse loading. After complete displacement, the von Mises residual stress distribution of the bent sheet is shown in Figure 14(b) by FEA. Plots for both the von Mises residual stress and equivalent plastic strain are shown in Figures 15 and 16, indicating that the von Mises stress in the thick area is higher than that in the thin area. Additionally, the residual stress and plastic strain are mainly concentrated in three locations, and the maximum plastic strain is in the middle position.
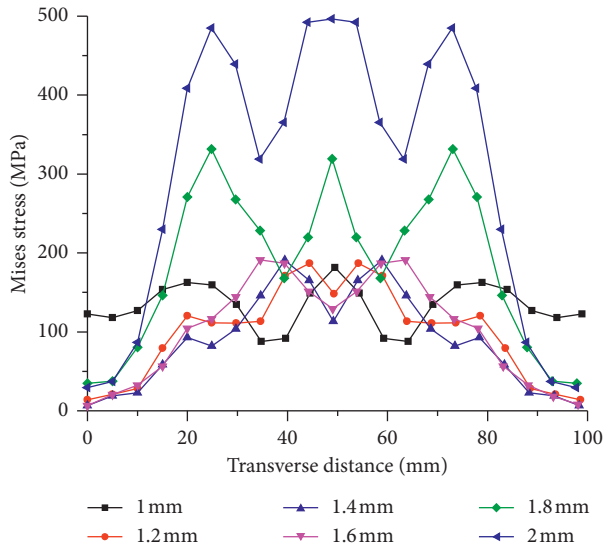
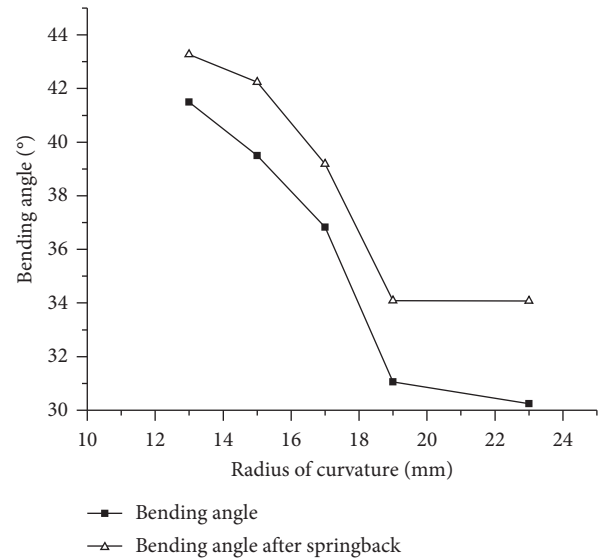FIGURE 15: Curves of von Mises stress after springback.

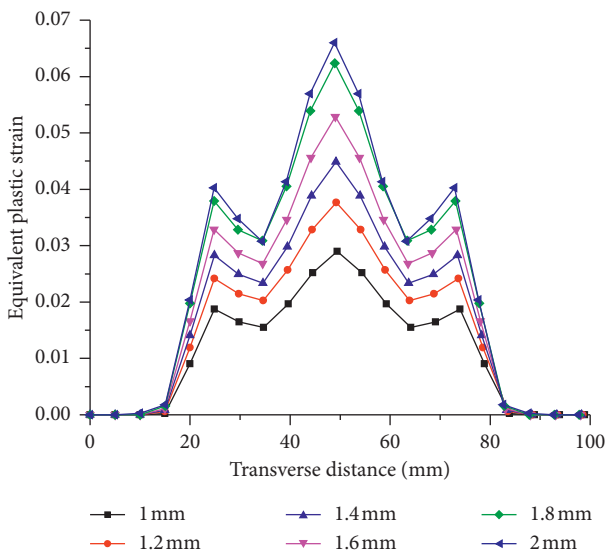FIGURE 16: Curves of equivalent plastic strain after springback.

FIGURE 17: Curves of von Mises stress after springback.

3.2. Effects of Forming Parameters on Springback in Cylindrical Bending of TRB.

The cylindrical bending process of the TRB has formation parameters that change the bending angle and springback characteristics. One of these formation parameters is varied individually, and all of the other parameters are fixed to the values of the base case ($\rho = 19$ mm, $R = 8$ mm, and $t/T = 0.8$) to investigate the effects of the parameters on the bending angle. All of the formation parameters are controlled within a range of values considering the practical formation process. The main cylindrical bending parameters influencing the bending shape are the radius of curvature ρ ($\rho = R_p/2 + R_d/2$), die corner radius (R), and TRB thickness ratio (t/T). First, the radius of curvature (R) is varied, while the die radius (R_d) and the TRB thickness ratio (t/T) are kept at $R = 8$ mm and $t/T = 0.8$, respectively. Figure 17 shows a plot of the bending angle before and after springback as a function of the radius of curvature (ρ). As the radius of curvature (ρ) increases, the bending angle after springback drops sharply compared with that before springback, causing deformation to rise sharply. This results in the bending angle before and after springback reaching an inflection point at $\rho = 19$ mm. A greater increase in R leads to gradually less improvement in the bending angle.

The effect of the radius of curvature (ρ) on the springback angle on the base case $R = 8$ mm and $t/T = 0.8$ is illustrated in Figure 18. It was found that the springback angle varies approximately linearly with the radius of curvature (ρ), and variation from $\rho = 13$ mm to $\rho = 23$ mm can produce a springback angle from 1.8° to 3.8°, which means that more deformation occurs in a larger radius of curvature (ρ), and more deformation leads to more springback. Therefore, a larger radius of curvature (R) provides significant springback.

Figure 19 demonstrates the influence of the die corner radius R on the bending angles before and after springback. As the die corner radius R increases from 4 mm to 8 mm, the bending angles before and after springback increase by approximately 15°. At the same time, the springback angle is slightly reduced, from 3.8° to 3° with the increase in the die corner radius R from 4 mm to 8 mm, as shown in Figure 20. It is concluded that a larger die corner radius R can be helpful to improve bending angles and reduce the springback angle.

To study the effect of the thickness transition zone of the TRB on the springback, the thickness ratio (t/T) of the thick region and the thin region in the TRB is defined to evaluate the thickness gradient. The corresponding cylindrical bending process of TRB is calculated and shown in Figures 21 and 22. As the TRB thickness ratio (t/T) increases, the bending angles are seen to increase at a low rate nearly linearly with t/T, but the springback angle is significantly increased from 3.5° to 4.3°. Thus, the TRB thickness ratio (t/T) is a major factor influencing the springback angle but has little effect on the bending angle.
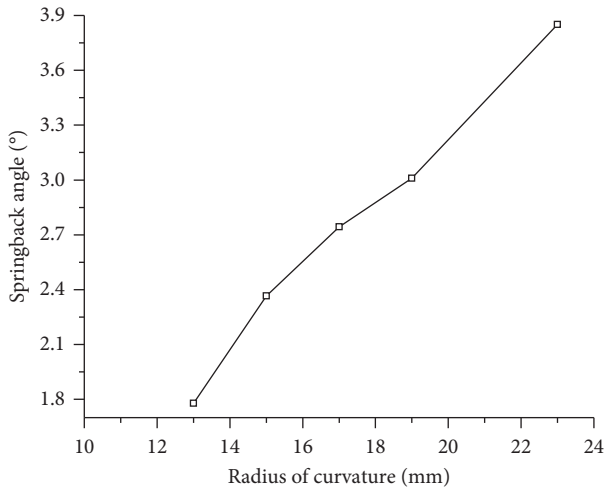
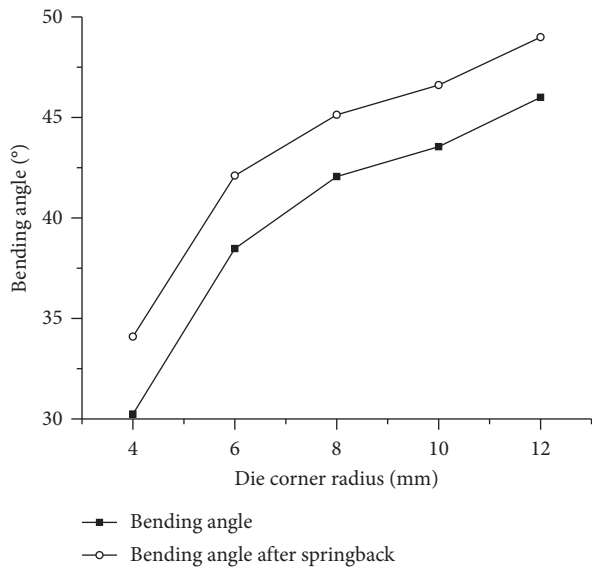Figure 18: Curves of equivalent plastic strain after springback.

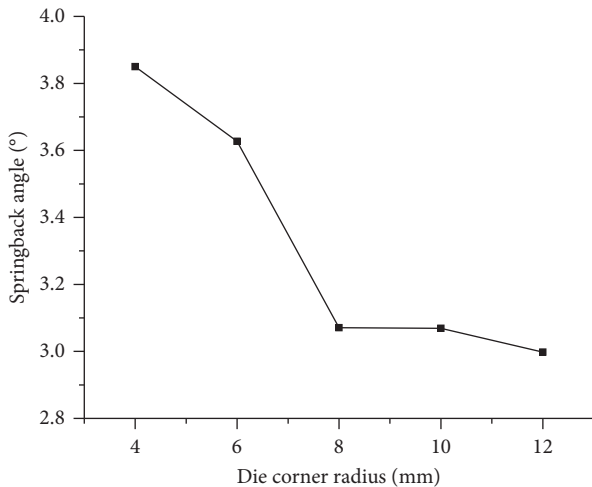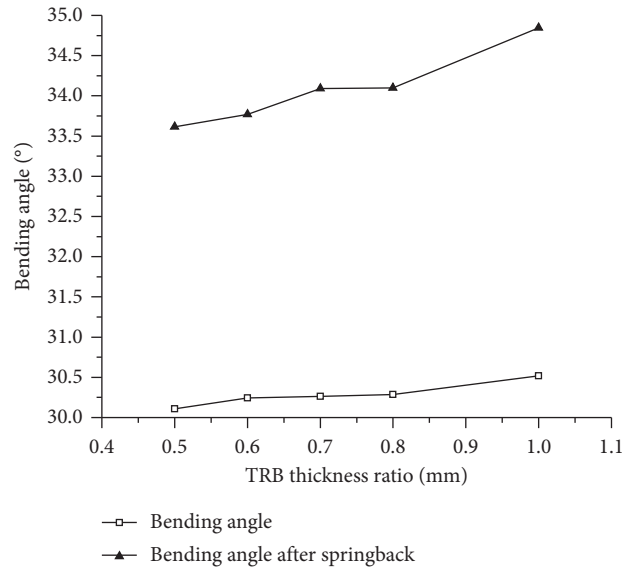Figure 21: Curves of von Mises stress after springback.

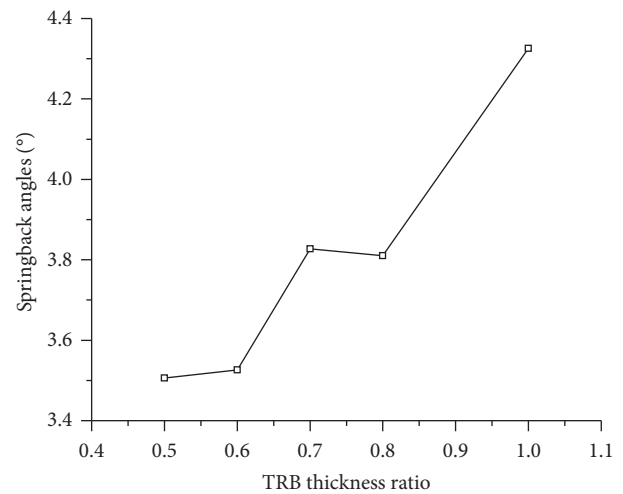Figure 19: Curves of von Mises stress after springback.

Figure 22: Curves of equivalent plastic strain after springback.

4. Conclusions

In this study, a simulation model for the cylindrical bending process of TRBs is constructed. To describe the gradient of the mechanical properties with the TRB thickness, the user subroutine USDFLD programmed in FORTRAN is used to build the material model. The deformation behaviours in the cylindrical bending process of the TRB are calculated. A parametric study of the cylindrical bending process of TRBs is conducted to analyse the effects of the formation parameters on the bending angle and springback angle. The following conclusions can be made:

(1) The simulated bending angle before and after springback of the TRB showed good agreement with the experimental results. The simulation model incorporating the gradient of mechanical properties with the TRB thickness can predict springback in cylindrical bending very well.

Figure 20: Curves of equivalent plastic strain after springback.

(2) The cylindrical bending of the TRB process gradually evolved from three-point bending to four-point bending and, finally, to multipoint bending. The thickness gradient leads to the nonuniform longitudinal distribution of the von Mises stress.

Larger bending angles can be achieved by reducing R and improving R_d, but t/T has little effect on the bending angles. In terms of the influence of springback, increasing R_d and reducing R and t/T can lead to a smaller springback angle.

Data Availability

The data sets supporting the conclusions of this article are included within the article.

Conflicts of Interest

The authors declare that they have no conflicts of interest.

Acknowledgments

References

[1] R. Kopp, C. Wiedner, and A. Meyer, "Flexibly rolled sheet metal and its use in sheet metal forming," *Sheet Metal 2005*, vol. 6–8, pp. 81–92, 2005.

[2] G. Hirt and D. H. Dávalos-Julca, "Tailored profiles made of tailor rolled strips by roll forming—part 1 of 2," *Steel Research International*, vol. 83, no. 1, pp. 100–105, 2012.

[3] P. Groche and M. Mirtsch, "Tailored profiles made of tailor rolled strips by roll forming—part 2 of 2," *Steel Research International*, vol. 83, no. 1, pp. 106–114, 2012.

[4] C. Huang, Y. Gan, J. T. Du, C. Z. Chen, and Q. J. Chen, "Shape rolling simulation of tailor rolled blanks based on deform-3D," *Applied Mechanics and Materials*, vol. 101-102, pp. 897–900, 2011.

[5] H. J. Jiang and H. L. Dai, "A novel model to predict U-bending springback and time-dependent springback for a HSLA steel plate," *International Journal Advance Manufacture Technology*, vol. 81, no. 5–8, pp. 1055–1066, 2015.

[6] N. Nanu and G. Brabie, "Analytical model for prediction of springback parameters in the case of U stretch-bending process as a function of stresses distribution in the sheet thickness," *International Journal Mechanical Science*, vol. 64, no. 1, pp. 11–21, 2012.

[7] X. Yang, C. Choi, N. K. Sever, and T. Altan, "Prediction of springback in air-bending of advanced high strength steel (DP780) considering Young's modulus variation and with a piecewise hardening function," *International Journal of Mechanical Sciences*, vol. 105, no. 105, pp. 266–272, 2016.

[8] G. L. Quilliec, P. Breitkopf, J. M. Roelandt, and P. Juillard, "Semi analytical approach for plane strain sheet metal forming using a bending-under-tension numerical model," *International Journal of Material Forming*, vol. 7, no. 2, pp. 221–232, 2014.

[9] M. G. Lee, D. Kim, R. H. Wagoner, and K. Chung, "Semi-analytic hybrid method to predict springback in the 2D draw bend test," *Journal of Applied Mechanics*, vol. 74, no. 6, pp. 1264–1275, 2007.

[10] S. K. Panthi and N. Ramakrishnan, "Semi analytical modeling of springback in arc bending and effect of forming load," *Transactions of Nonferrous Metals Society of China*, vol. 21, no. 10, pp. 2276–2284, 2011.

[11] B. Chongthairungruang, V. Uthaisangsuk, S. Suranuntchai, and S. Jiratheanarat, "Experimental and numerical investigation of springback effect for advanced high strength dual phase steel," *Materials & Design*, vol. 39, pp. 318–328, 2012.

[12] C. Q. Guo, J. Chen, J. S. Chen, D. K. Xu, X. Y. Yu, and Y. C. Bai, "Numerical simulation and experimental validation of distortional springback of advanced high-strength steel sheet metal forming," *Journal Shanghai Jiaotong University*, vol. 4, 2010.

[13] H. Kim and M. Kimchi, "Numerical modeling for springback predictions by considering the variations of elastic modulus in stamping advanced high-strength steels (AHSS)," in *Proceedings of the 8th International Conference Work Number Simulation 3D sheet Meeting Form Process*, pp. 1159–1166, Melville, NY, USA, August 2011.

[14] H. W. Zhang, X. H. Liu, L. Z. Liu, P. Hu, and J. L. Wu, "Study on nonuniform deformation of tailor rolled blank during uniaxial tension," *Acta Metallurgica Sinica (English Letter)*.vol. 28, no. 9, pp. 1198–1204, 2012.

[15] S. Zhang, X. Liu, and L. Liu, "Characterization of stress-strain relationship of tailor rolled blank's thickness transition zone," *Journal of Mechanical Engineering*, vol. 54, no. 18, pp. 49–54, 2018.

[16] H. W. Zhang, L. Z. Liu, and P. Hu, "Springback characteristics in U-channel forming of tailor rolled blank," *Acta Metallurgica Sinica (English. Letters)*, vol. 25, no. 3, pp. 207–213, 2012.

[17] A. Meyer, B. Wietbrock, and G. Hirt, "Increasing of the drawing depth using tailor rolled blanks—numerical and experimental analysis," *International Journal of Machine Tools & Manufacture*, vol. 48, no. 5, pp. 522–531, 2008.

[18] J.-H. Kim, C.-J. Lee, S.-B. Lee, D.-C. Ko, and B.-M. Kim, "Integrated hot forming and heat treatment process on Al6061 tailor rolled blank," *International Journal of Precision Engineering and Manufacturing*, vol. 18, no. 1, pp. 127–132, 2017.

[19] G. H. Shim, J. H. Kim, and B. M. Kim, "Springback prediction of tailor rolled blank in hot stamping process by partial heating," *Transactions of Materials Processing*, vol. 25, no. 6, pp. 396–401, 2016.

[20] R. Lu, X. Liu, Z. Xu, X. Hu, Y. Shao, and L. Liu, "Simulation of springback variation in the U-bending of tailor rolled blanks," *Journal of the Brazilian Society of Mechanical Sciences and Engineering*, vol. 39, no. 11, pp. 4366–4647, 2017.